Photosynthesis, leaf hydraulic conductance and embolism dynamics in the resurrection plant Barbacenia purpurea

Miquel Nadal, Marc Carriquí, Eric Badel, Hervé Cochard, Sylvain Delzon, Andrew King, Laurent J Lamarque, Jaume Flexas, José M Torres-ruiz

Received: 24 May 2023 | Revised: 17 August 2023 | Accepted: 15 September 2023

DOI: 10.1111/ppl.14035

ORIGINAL RESEARCH

Physiologia Plantarum

Photosynthesis, leaf hydraulic conductance and embolism dynamics in the resurrection plant *Barbacenia purpurea*

Miquel Nadal[1,2] | Marc Carriquí[2,3] | Eric Badel[4] | Hervé Cochard[4] | Sylvain Delzon[5] | Andrew King[6] | Laurent J. Lamarque[5] | Jaume Flexas[2] | José M. Torres-Ruiz[4]

[1]Departamento de Sistemas Agrícolas, Forestales y Medio Ambiente, Centro de Investigación y Tecnología Agroalimentaria de Aragón (CITA), Zaragoza, Spain

[2]Research Group on Plant Biology under Mediterranean Conditions, Universitat de les Illes Balears (UIB), Institut d'Investigacions Agroambientals i d'Economia de l'Aigua (INAGEA), Palma, Illes Balears, Spain

[3]Instituto de Ciencias Forestales (ICIFOR-INIA), CSIC, Madrid, Spain

[4]Université Clermont-Auvergne, INRAE, PIAF, Clermont-Ferrand, France

[5]Université de Bordeaux, INRAE, BIOGECO, Pessac, France

[6]Synchrotron Source Optimisée de Lumière d'Energie Intermédiaire du LURE, L'Orme de Merisiers, France

Correspondence
Miquel Nadal, Departamento de Sistemas Agrícolas, Forestales y Medio Ambiente, Centro de Investigación y Tecnología Agroalimentaria de Aragón (CITA), Avda. Montañana 930, Zaragoza 50059, Spain.
Email: m.n.nadal92@gmail.com

Funding information
Ministerio de Ciencia e Innovación, Grant/Award Numbers: FJC2020-042856-I, FJC2020-043902-I; Ministerio de Ciencia, Innovación y Universidades, Grant/Award Number: PGC2018-093824-B-C41; Ministerio de Economía y Competitividad, Grant/Award Number: BES-2015-072578; Région Auvergne-Rhône-Alpes 'ThirsTree', Grant/Award Numbers: 20-006175-01, 20-006175-02

Edited by Y. Utsumi

Abstract

The main parameters determining photosynthesis are stomatal and mesophyll conductance and electron transport rate, and for hydraulic dynamics they are leaf hydraulic conductance and the spread of embolism. These parameters have scarcely been studied in desiccation-tolerant (resurrection) plants exposed to drought. Here, we characterized photosynthesis and hydraulics during desiccation and rehydration in a poikilochlorophyllous resurrection plant, *Barbacenia purpurea* (Velloziaceae). Gas exchange, chlorophyll fluorescence, and leaf water status were monitored along the whole dehydration-rehydration cycle. Simultaneously, embolism formation and hydraulic functioning recovery were measured at leaf level using micro-computed tomography imaging. Photosynthesis and leaf hydraulic conductance ceased at relatively high water potential (−1.28 and −1.54 MPa, respectively), whereas the onset of leaf embolism occurred after stomatal closure and photosynthesis cessation (<−1.61 MPa). This sequence of physiological processes during water stress may be associated with the need to delay dehydration, to prepare the molecular changes required in the desiccated state. Complete rehydration occurred rapidly in the mesophyll, whereas partial xylem refilling, and subsequent recovery of photosynthesis, occurred at later stages after rewatering. These results highlight the importance of stomata as safety valves to protect the vascular system from embolism, even in a plant able to fully recover after complete embolism.

Miquel Nadal and Marc Carriquí contributed equally to this work.

1 | INTRODUCTION

Desiccation-tolerant or "resurrection" plants are a distinct group of species that are able to tolerate and recover from extreme water loss in their vegetative tissues. Desiccation tolerance in these species is defined as the capacity to survive drying to a water potential (Ψ) of approximately −100 MPa, equivalent to achieving equilibrium with a relative air humidity of 50% at 20°C (Alpert, 2005). These conditions result in a leaf water content of approximately 0.1 g g^{-1}, and a relative water content (RWC) below 10% (Alpert, 2005). Desiccation tolerance is widespread among bryophytes (Oliver et al., 2005; Wood, 2007), and it has evolved independently several times among vascular plants (Gaff & Oliver, 2013; Oliver et al., 2000): there are about 140 angiosperm species described as desiccation-tolerant (Fu et al., 2022; Gaff & Oliver, 2013), and a larger number of about >200 ferns (Porembski, 2011). The mechanisms of desiccation tolerance include sugar and late embryogenesis abundant proteins (LEAs) accumulation, antioxidant activity, leaf and cell wall folding, cytosol vitrification, and vacuole fragmentation, among others (see Oliver et al., 2020). The most derived type of desiccation tolerance is found in poikilochlorophyllous resurrection plants, which dismantle chlorophyll together with chloroplasts and their photosynthetic machinery in the desiccated state and resynthesize it upon rehydration (Fernández-Marín et al., 2016). This extreme mechanism allows them to survive for extended periods of about 5–10 months in the complete absence of water, with minimum oxidative damage (Tuba, 2008). On the contrary, homoiochlorophyllous resurrection plants retain and mask chlorophyll in the desiccated state (Oliver et al., 2020).

Photosynthesis is a relatively sensitive process to water stress. Hsiao et al. (1976) already reported that CO_2 uptake was limited at leaf water potentials between −1 and −2 MPa, well above the −4 to −5 Mpa considered as lethal for leaves in the majority of desiccation-sensitive species (Lens et al., 2022; Oliver et al., 2020). In terms of relative water content (RWC), full cessation of net CO_2 assimilation (A_n) and stomatal conductance (g_s) has been reported in the 98%–50% range among vascular plants (Perera-Castro et al., 2020; Trueba et al., 2019), being much higher than the values reported for triggering most mechanisms associated with desiccation tolerance (~30% RWC; Farrant & Moore, 2011). Photosynthesis decline under water stress is driven by a combination of diffusion and biochemical constraints (Chaves et al., 2009; Flexas et al., 2004; Nadal & Flexas, 2019). CO_2 diffusion limitations include reduction of g_s due to stomatal closure upon dehydration and decreases in mesophyll conductance (g_m), where the latter comprises the CO_2 diffusion path from the substomatal chamber to the sites of carboxylation in the chloroplasts (Evans et al., 2009; Flexas et al., 2008; Nadal & Flexas, 2018). Biochemical and photochemical limitations to photosynthesis, which include the electron transport rate (J_{flu}) in the thylakoids, the maximum carboxylation rate by Rubisco ($V_{c,max}$), and RuBP regeneration in the Calvin cycle (Gago et al., 2019), occur under prolonged water stress (Galmés et al., 2007; Galmés et al., 2011). Leaf hydraulic conductance (K_{leaf}) also influences photosynthesis decline as concomitant K_{leaf} and transpiration reduction during water stress directly influence turgor pressure, leading to g_s decline (Rodríguez-Domínguez et al., 2016; Wang et al., 2018).

One of the main causes of K_{leaf} decline under drought is the formation of embolisms in the xylem conduits. Thus, when tensions in the xylem exceed a critical threshold, air enters into the conduit lumen. If embolism events become massive, the water transport through the leaf can be blocked due to hydraulic disfunction. To delay such embolism formation and fatal dehydration for the surrounding tissues (Brodribb et al., 2021; Mantova et al., 2022), plants close their stomata to reduce water losses at the cost of reducing their carbon assimilation. In fact, recent studies have shown how stomatal closure occurs before, that is, at higher water potentials, than the onset of leaf embolism (Corso et al., 2020; Creek et al., 2020; Hochberg et al., 2017; Skelton et al., 2017). Therefore, the safety margin, that is, the difference in water potential between stomatal closure and embolism, is a key trait in drought tolerance (Chen et al., 2019; Creek et al., 2020; Martin-StPaul et al., 2017). However, other studies indicate that embolism is partially responsible for stomatal closure and that an overlap exists between g_s decline and xylem loss of conductivity along the Ψ gradient (Bartlett et al., 2016; Savi et al., 2016; Torres-Ruiz et al., 2015a; Trifilò et al., 2015; Zufferey et al., 2011). In this sense, given the ability of resurrection plants to recover after extensive water loss, they provide an intriguing system to test the coordination between stomatal response and embolism spread in leaves. Most notably, Prats and Brodersen (2021) reported a decoupling between photosynthesis and water transport in the leaf of the resurrection fern *Pleopeltis polypodioides*, where photosynthesis declined by only half just after complete embolism of the stipe xylem.

Few studies have investigated the dynamics of the hydraulic system of resurrection plants during dehydration and rehydration. Sherwin et al. (1998) described the embolism events using the acoustic technique in the stem of the only known woody resurrection plant, *Myrothamnus flabellifolius*, and showed that its vessels remained completely embolised in the desiccated state. Leaves and stems in *M. flabellifolius* lost water at a similar water potential when the bulk of embolism events occurred, suggesting that plants do not "prevent" extensive embolisms and use all available water during desiccation (Sherwin et al., 1998). The hydraulic functioning dynamics of the xylem have been characterized using X-ray micro-computed tomography (microCT), a non-invasive technique for quantifying xylem embolism in intact plants (Choat et al., 2016; Torres-Ruiz et al., 2015b). In petioles of the desiccation-tolerant fern *Pentagramma triangularis* (Holmlund et al., 2019), x-ray images showed how tracheid embolism occurred prior to dehydration of the accompanying living tissues within the vascular cylinder. Studies in these species have also provided some mechanisms for xylem refilling during rehydration: both positive root pressure and capillary ascension of water have been suggested to play a significant role in the rehydration of the vascular system (Schneider et al., 2000; Sherwin et al., 1998), and possibly a distinct cell wall composition enhances the wettability of the desiccated tissue (Holmlund et al., 2019). Recently, Prats and Brodersen (2021) explored the coordination of xylem embolism refilling using microCT and photosynthesis in the resurrection fern *P. polypodioides*,

showing that full embolism repair in the stipe was not required for photosynthesis recovery. To date, only Fu et al. (2022) have simultaneously characterized photosynthesis and water relation dynamics during both dehydration and rehydration in the resurrection angiosperm *Paraboea rufescens*. Notably, they found that leaf gas exchange recovered at a slower rate than water status during rehydration (McAdam & Brodribb, 2012).

Barbacenia purpurea Hooker (Velloziacaeae, Monocot) is a poikilochlorophyllous resurrection plant from tropical and subtropical forests in Brazil, which inhabits rocky outcrops exposed to frequent drought periods (Meireles et al., 1997). The gas exchange, molecular, metabolomic, and cell wall response of *B. purpurea* has been characterized in response to water stress and recovery (Aidar et al., 2010, 2014; Suguiyama et al., 2014, 2016), and hence this species is a good model to explore the photosynthetic and hydraulic response in a resurrection plant.

In this study, we characterized the photosynthetic parameters, K_{leaf}, and embolism dynamics along a dehydration and rehydration cycle in *B. purpurea*. The main objectives were (1) to determine the sequence of physiological events like stomatal closure, photosynthesis shutdown, and embolism formation during desiccation in *B. purpurea* and (2) to explore the dynamics of recovery of xylem hydraulic function and photosynthesis during rehydration. We hypothesized that (1) even in the poikilochlorophyllous resurrection plant *B. purpurea*, stomatal closure would occur prior to the formation of embolisms in the xylem conduits and (2) the rate of leaf gas exchange recovery during rehydration would be hindered by a combination of chlorophyll re-synthesis and hydraulic recovery, unlike the previous reports of rapid photosynthesis recovery in resurrection ferns by Prats and Brodersen (2021).

2 | MATERIALS AND METHODS

Barbacenia purpurea plants were grown from seeds under glasshouse and natural irradiance conditions in the Universitat de les Illes Balears (Mallorca, Spain) in 2 l pots containing a 1:2 mixture of horticultural substrate and perlite for one year. Plants were kept well-irrigated and watered weekly with half-strength Hoagland's solution (Hoagland & Arnon, 1950). Two weeks prior to the beginning of the experiment, plants were transferred to a growth chamber at 25/20°C of day/night temperature and a photoperiod of 12/12 h with a photosynthetic photon flux density of ~400 µmol m^{-2} s^{-1}. For the characterization of the gas exchange, chlorophyll fluorescence, and leaf hydraulic conductance dynamics, a water stress treatment was imposed by withholding water for three weeks, the amount of time required to ensure that the desiccated state was induced in all plants. Then, plants were rehydrated repeating the pre-drought irrigation scheme and monitored for 1 week for recovery. Ten different individuals were used for all measurements along the dehydration and rehydration cycle to minimize damaging effects of leaf water status monitoring. Another subset of six plants was used for the embolism vulnerability characterization. These plants were grown under the same conditions as the aforementioned individuals and sent via express shipping (1-day travel) to the SOLEIL synchrotron (France) for x-ray micro-computed tomography (micro-CT) measurements.

2.1 | Gas exchange and photosynthesis

An open gas exchange system with a coupled fluorescence chamber of 2 cm^2 (LI-6400XT; LI-COR Inc.) was used to perform daily instantaneous measurements of gas exchange and chlorophyll fluorescence in leaves from 4 to 10 plants along the dehydration and rehydration cycle. Corrections for the leakage of CO_2 into and out of the LI-6400 chamber were applied to gas-exchange data following Flexas et al. (2007). Net CO_2 assimilation (A_n), transpiration rate I, stomatal conductance to water vapor (g_{sw}), and photochemical yield of photosystem II (Φ_{PSII}) were recorded after reaching steady-state conditions (5–10 min) at ambient CO_2 (400 µmol mol^{-1}), saturating photosynthetic photon flux density (*PPFD*; 1250 µmol m^{-2} s^{-1}), ambient relative humidity (50–70%) and 25°C block temperature. All g_{sw} values were corrected for residual conductance to water vapor (g_{res}) as in Théroux Rancourt et al. (2015) to calculate stomatal conductance to CO_2 (g_{sc}) and substomatal CO_2 concentration (C_i). g_{res} was measured in six detached leaves subjected to dehydration in the lab at a controlled temperature (25°C) following Sack and Scoffoni (2011). At 2–3 day intervals along the dehydration and rehydration cycle, light curves were performed under non-photorespiratory conditions (O_2 < 2%) to obtain estimations of mitochondrial respiration in the light (R_l) and the fraction of *PPFD* harvested by PSII (s) following the procedures described in Bellasio et al. (2016). The electron transport rate measured from chlorophyll fluorescence (J_{flu}) was calculated for instantaneous measurements as $J_{flu} = PPFD \cdot s \cdot \Phi_{PSII}$ (Bellasio et al., 2016). Mesophyll conductance to CO_2 (g_m) was estimated from instantaneous measurements using the variable J method (Harley et al., 1992) where $g_m = A_n/(C_i - \Gamma^* \cdot (J_{flu} + 8 \cdot (A_n + R_l))/(J_{flu} - 4 \cdot (A_n + R_l)))$. The CO_2 compensation point in the absence of respiration (Γ^*) was estimated from the combination of the A/C_i curves performed under ambient and low O_2 in well-watered plants as described in Bellasio et al. (2016). The mean value of Γ^* obtained under well-watered conditions was used for all the dehydration and rehydration measurements as in vivo methods are prone to artifacts under water stress (Galmés et al., 2006).

Additionally, the maximum yield of PSII (F_v/F_m) was measured daily in 1-h dark-acclimated leaves from 4 to 6 plants using a Junior-PAM fluorimeter (Heinz Walz GmbH).

2.2 | Water status

Plant water status was monitored by measuring leaf water potential at predawn (Ψ_{pd}) and stem (Ψ_{stem}) and leaf (Ψ_{leaf}) water potential at midday every 2 days during water stress and every day during recovery. Due to the limited number of leaves per individual, each water potential was measured in 4–8 leaves from different plants every time using

a Scholander pressure chamber (Model 600D; PMS Instrument Company). Ψ_{stem} was measured from equilibrated leaves covered for 2 h prior to sampling at midday. Relative water content (RWC) and Ψ_{leaf} were measured after instantaneous gas exchange measurements in the same leaves. Quickly after the gas exchange, leaves were excised, equilibrated for 10–15 min in the dark with sealed plastic bags under high humidity conditions, measured for water potential, and subsequently weighted and rehydrated overnight for obtaining the fresh (FW) and turgid weights (TW), respectively. Dry weight (DW) was then determined after at least 72 h at 70°C. RWC was calculated as RWC = (FW−DW)/(TW−DW) × 100. In addition, soil water content was tracked daily using a humidity probe (WET-2 Sensor/HH2 Moisture Meter, Delta-T Devices).

2.3 | Hydraulic conductance

Leaf hydraulic conductance (K_{leaf}) was calculated from instantaneous gas exchange and water status measurements performed along the dehydration and rehydration cycle using the in vivo evaporative flux method (Tsuda & Tyree, 2000), where $K_{leaf} = E/(\Psi_{stem}-\Psi_{leaf})$. Ψ_{stem} and Ψ_{leaf} were measured in the same individual, and E was taken from LI-6400XT measurements. Measured E was assumed as representative of whole-leaf E (Théroux Rancourt et al., 2015). To confirm the reliability of in vivo K_{leaf} measurements in attached leaves, K_{leaf} was also measured with the evaporative flux method in excised leaves ($n = 24$) subjected to saturating photosynthetic photon flux density ($PPFD$ > 1250 µmol m^{-2} s^{-1}) and to different degrees of dehydration from well-watered individuals as described in Sack and Scoffoni (2012). Briefly, leaves were connected through a sealed tube to sonicated distilled water, and whole-leaf E under saturating light was determined gravimetrically in a well-ventilated room at 25°C. Final Ψ_{leaf} was measured with the pressure chamber after a 10–15 min. equilibration.

2.4 | Direct visualization of embolism spread using x-ray microCT

The direct, non-invasive visualization of xylem embolism of *B. purpurea* was performed using the High-Resolution X-ray microCT facility available in the PSICHE beamline of the synchrotron SOLEIL (Saclay, France; King et al., 2016). Six well-watered potted plants were allowed to progressively dehydrate for 1 week by withholding the irrigation right before the experiment. During dehydration, two to three leaves per plant were scanned at different times (one to three days apart) in order to have a range of different water potentials. Scans were performed on leaves that were attached to the rest of the plant, that is, not in excised leaves. The resolution of each scan was 0.87 μm^3 and samples were scanned using a high flux (3.1011 photons mm^{-1}) 25-keV monochromatic x-ray beam and a continuous rotation from 0^0 to 180^0. X-ray projections were collected with a 50 ms exposure time during rotation and recorded with an Orca-flash sCMOS camera (Hamamatsu Photonics K.K.) equipped with a 250 µm-thick LuAG scintillator. The total scan time was about 3 min and resulted in a stack of 752 to 1024 TIFF image slices over 0.9 mm along the plant organ. Tomographic reconstructions were performed using the Paganin method (Paganin et al., 2002) in the PyHST2 software (Mirone et al., 2014) and resulted in 32-bit volume images. Right after the first scan, a second scan was performed for each leaf after cutting it in the air right above the scanned area, inducing air entry in the remaining functional vessels (Torres-Ruiz et al., 2015b) and therefore 100% of embolized vessels in the area (final cut). Leaf water

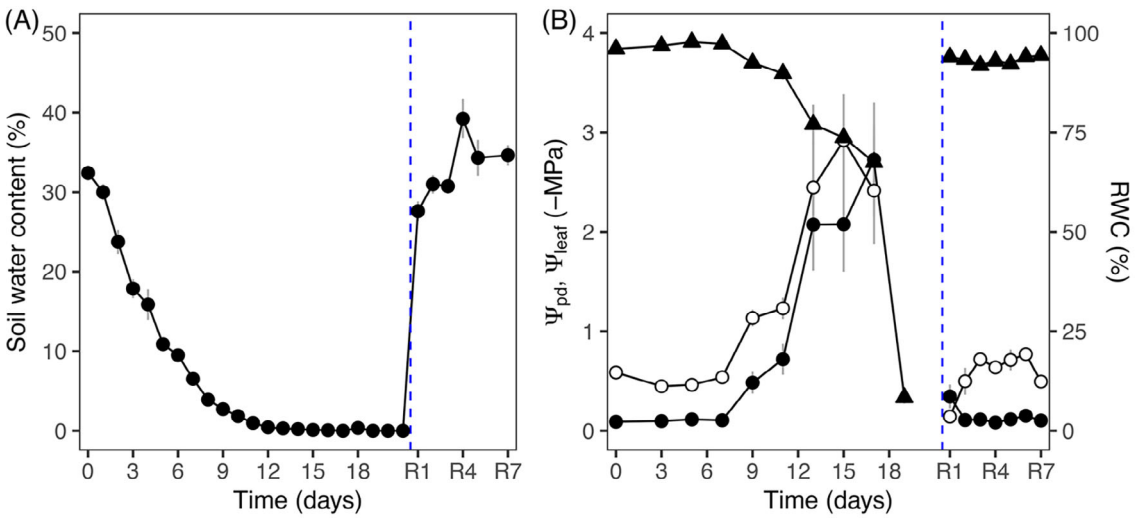

FIGURE 1 Pot and plant water status along the dehydration and rehydration cycle. (A) pot soil water content, (B) predawn water potential (Ψ_{pd}, closed circles), leaf water potential at midday (Ψ_{leaf}, open circles), and leaf relative water content (RWC, closed triangles). The "R" followed by a number on the x-axis represents the day after rehydration. Extreme dehydration after day 16 caused the leaf water potential to fall beyond the range of the pressure chamber (<−4 MPa). Symbols and error bars are means of 4–8 replicates ± SE. The dashed blue line indicates the day of rewatering for recovery (day 21).

potential was directly measured in the excised leaf portion (ca. 15-cm long) immediately after the cut with a Scholander pressure chamber (Model 1000, PMS Instrument, OR, and SAM Precis). At the end of the experiment, five out of the six measured plants were rehydrated to evaluate the first stages of recovery (4–16 h after rewatering). Similar scans as those explained above were carried out to check for the recovery of the hydraulic functioning. Overall, four to six leaves per plant were scanned during the whole dehydration and rehydration cycle and no leaf was scanned twice. For each leaf, the amount of embolized vessels was quantified by calculating the theoretical hydraulic conductivity of a whole scanned cross section (k_h^{th}) by determining the individual area and diameter of functional and

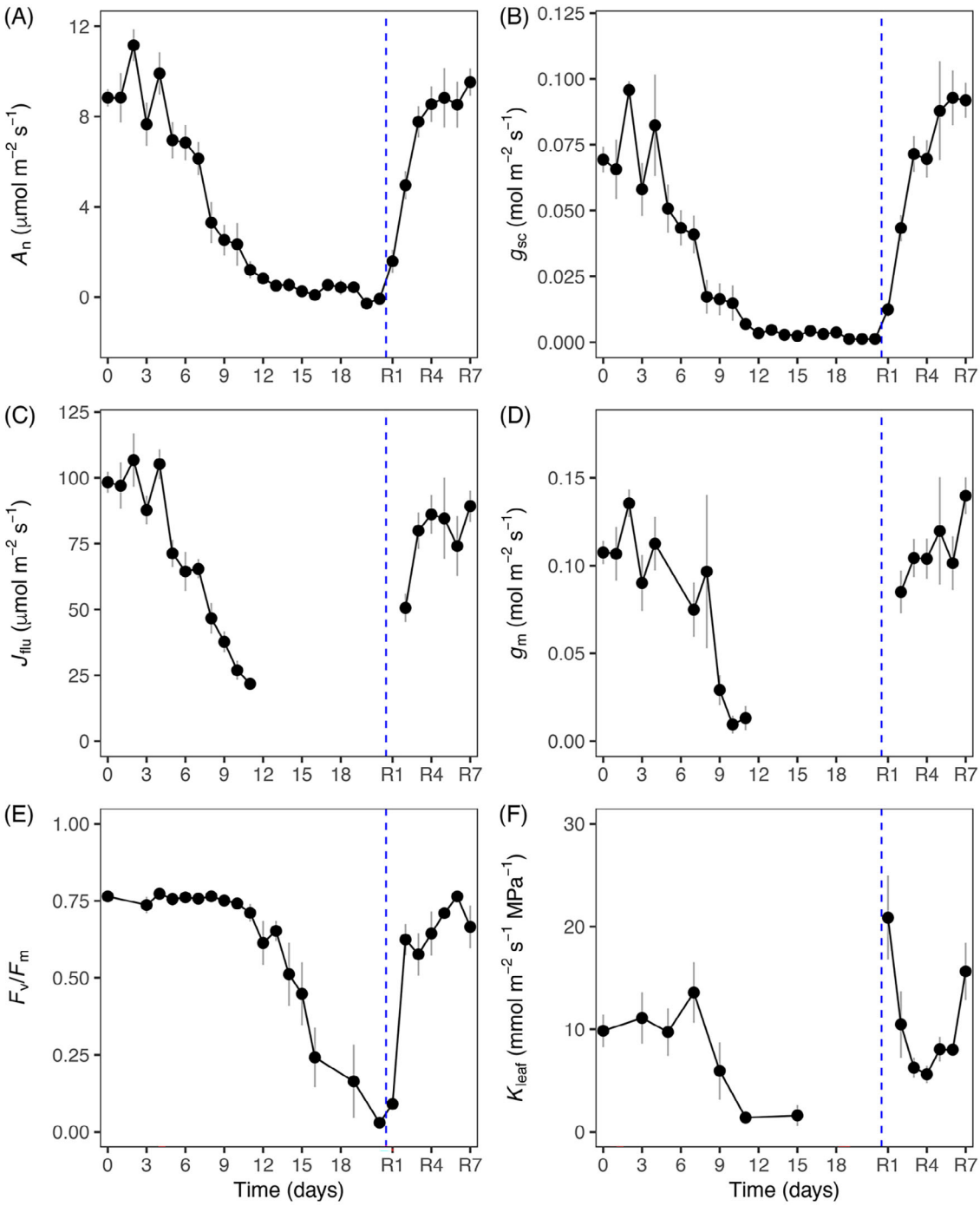

FIGURE 2 Photosynthesis response along the dehydration and rehydration cycle. (A) net CO_2 assimilation (A_n), (B) stomatal conductance to CO_2 (g_{sc}), (C) electron transport rate (J_{flu}), (D) mesophyll conductance to CO_2 diffusion (g_m), (E) maximum yield of PSII (F_v/F_m), (F) leaf hydraulic conductance (K_{leaf}). The "R" followed by a number on the x-axis represents the day after rehydration. Photosynthesis cessation did not allow for adequate measurement of J_{flu} and g_m during the later stages of dehydration. Circles and error bars are means of 4–10 replicates ± SE. The dashed blue line indicates the day of recovery (day 21).

embolised vessels using ImageJ software (Schneider et al., 2012). Thus, k_h^{th} (kg s^{-1} MPa^{-1}) of air-filled vessels of each intact leaf was calculated as $k_h^{th} = \Sigma \pi D^4/128 \eta$, where D is the diameter of the vessels (m) and η is the water viscosity (1.002×10^{-3} Pa s at 20°C). The theoretical percentage loss of the theoretical hydraulic conductivity (PLC) was then determined as PLC = 100 ($k_h^{th}/k_h^{th,max}$), where $k_h^{th,max}$ represents the theoretical hydraulic conductivity of all functional vessels as based on a cross section after the final cut.

2.5 | Pressure-Volume curves

Pressure-Volume (P-V) curves were performed following the bench-dry method (Sack & Pasquet-Kok, 2011) for six leaves from well-watered plants to determine the osmotic potential and relative water content at turgor loss point (π_{tlp} and RWC_{tlp}, respectively). Briefly, leaves were collected at predawn (initial $\Psi_{leaf} = 0.12 \pm 0.02$ MPa) and dehydrated in the lab, being alternatively weighted and measured for water potential until a complete P-V curve with at least 12 points was obtained. No oversaturation or "plateau" effect (Sack & Pasquet-Kok, 2011) was observed in any case. The identification of the turgor loss point was established considering the highest R^2 of a linear fit for the linear portion of the $-1/\Psi_{leaf}$ vs. 1–RWC relationship.

2.6 | Statistical analysis

The relationships between the studied parameters and Ψ_{leaf} were fitted using either linear, exponential, or sigmoidal models (Trueba et al., 2019) and the Akaike Information Criteria (AIC) was applied to select the most appropriate model. In almost all cases, the sigmoidal model presented the lowest AIC. The Weibull model, a variation of the

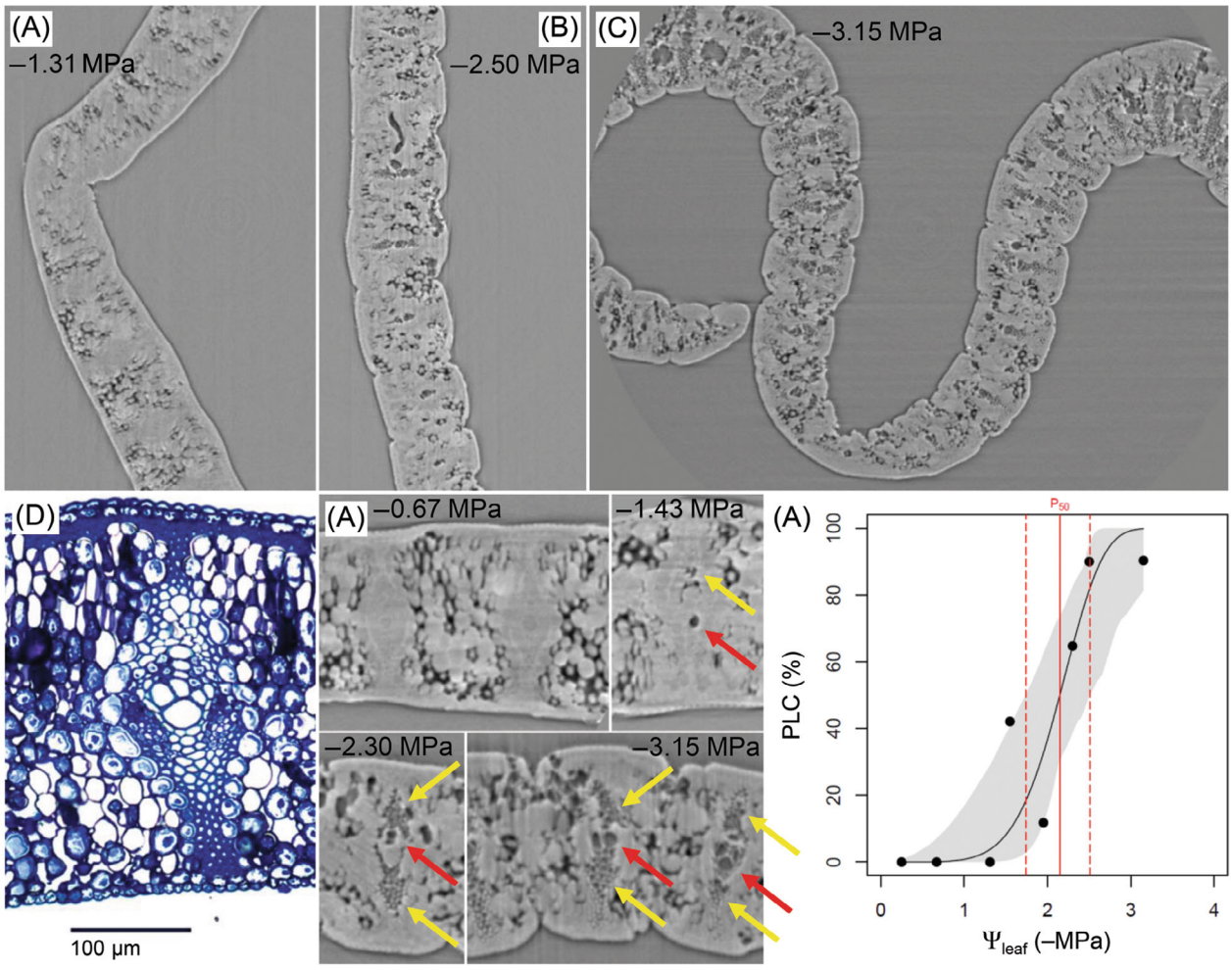

FIGURE 3 Leaf embolism during dehydration. (A–C) Representative x-ray microCT images of dehydrating leaves (leaf water potential, Ψ_{leaf}, is indicated for each image). (D) Light micrograph of a cross-section of a vascular bundle from a well-watered leaf; anatomical sample of *B. purpurea* from Nadal et al. (2021a). (E) Detail of vascular bundles from different leaves (Ψ_{leaf} is indicated for each image). Embolism of major vessels is indicated with red arrows, and of minor vessels with yellow arrows. (F) Hydraulic vulnerability curve represented as percentage loss of hydraulic conductivity (PLC) calculated using theoretical hydraulic conductivity (k_h^{th}) from microCT images. Data were fitted using the Weibull model; the gray shaded area represents the 95% bootstrapped confidence interval; the red solid line is the P_{50} (−2.15 MPa), and the dashed lines are its corresponding 95% confidence interval (1.73, 2.58). Calculated P_{12} and P_{88} are −1.61 and −2.60 MPa, respectively (see Table S1 for details).

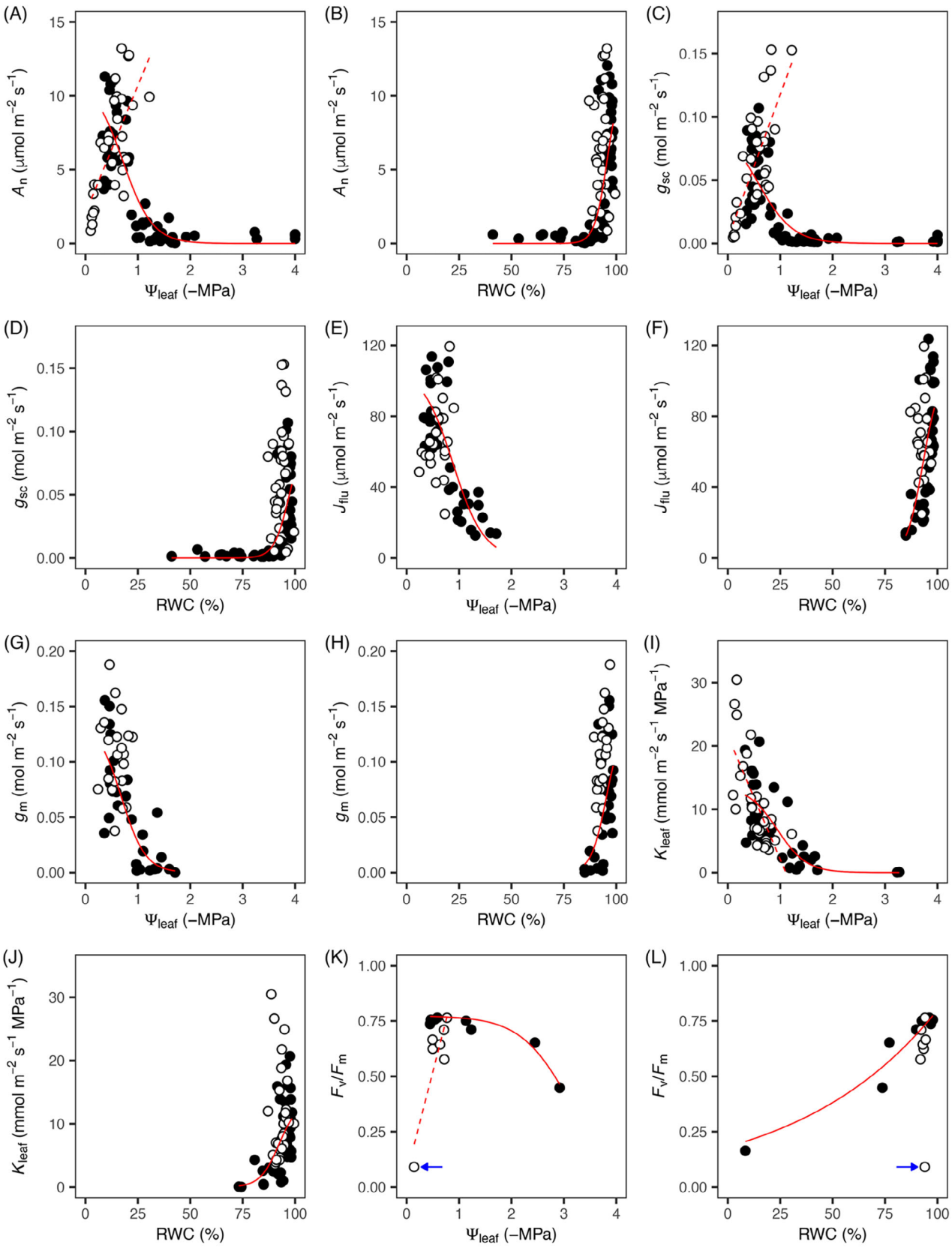

FIGURE 4 Relationships of photosynthesis and hydraulics with leaf water potential and relative water content. Circles represent individual leaves during dehydration (closed circles) and recovery (open circles). Lines denote significant ($p < 0.05$) fits for water stress (continuous; sigmoidal fitting) and recovery (dashed; linear fitting). Water potential at midday (Ψ_{leaf}) and relative water content (RWC) related to: (A,B) net CO_2 assimilation (A_n), (C,D) stomatal conductance to CO_2 (g_{sc}), (E,F) electron transport rate (J_{flu}), (G,H) mesophyll conductance to CO_2 (g_m), (I,J) leaf hydraulic conductance (K_{leaf}) measured in attached leaves, and (K,L) maximum yield of PSII (F_v/F_m), exponential fit for water stress; blue arrows indicate data point corresponding to the first day of recovery (12–24 h).

sigmoidal fitting, was used for PLC following Duursma and Choat (2017). The Ψ_{leaf} at which 12%, 50%, and 88% of PLC occurred (P_{12}, P_{50}, and P_{88}, respectively) was calculated by pooling together the data from the different plants. The Ψ_{leaf} and RWC at which 12%, 50%, and 88% decline occurred for A_n, J_{flu}, g_s, g_m, K_{leaf}, and F_v/F_m were calculated as described for PLC. All analyses were performed using the R statistical software (R Core Team, 2022). For non-linear fittings, the functions nls () and SSlogis() from the "stats" package were used. Confidence intervals for non-linear fittings were calculated using the fitplc() and fitcond() functions from the "fitplc" package (Duursma & Choat, 2017) and the predictNLS() function from the "propagate" package (Spiess, 2018).

3 | RESULTS

3.1 | Plant dehydration dynamics

Water deprivation led to a steep decrease in pot soil water content from an initial 32% to approximately 0% in 12 days (Figure 1A). Decreasing soil moisture imposed a reduction in predawn and midday leaf water potential (Ψ_{pd} and Ψ_{leaf}, respectively) and relative water content (RWC) on the 9th day of watering withholding (Figure 1B). As soil water content approached zero, the decrease in water status became more acute, with plants presenting $\Psi_{leaf} < -2$ MPa and RWC < 80% by the 13th day. All stressed plants reached the desiccated state (RWC < 10%) by the 19th day.

Most gas exchange parameters followed a similar pattern to that of the water potential and RWC, as leaves showed a decrease in net assimilation (A_n), electron transport rate (J_{flu}), stomatal conductance to CO_2 (g_{sc}), and mesophyll conductance to CO_2 (g_m) by the 8-9th day after water deprivation (Figure 2A–D). A_n and g_{sc} reached values near 0 by the 12th day (Figure 2A,B). Cessation and recuperation of photosynthesis were immediately followed by the decrease and recovery of F_v/F_m (Figure 2E). Similar to photosynthetic parameters, leaf hydraulic conductance (K_{leaf}) declined during the second week of water stress (Figure 2F). K_{leaf} assessed with the evaporative flux method in vivo and in excised leaves yielded comparable values under well-watered conditions (9.85 ± 1.59 and 10.91 ± 1.99 mmol m^{-2} s^{-1} MPa^{-1}, respectively).

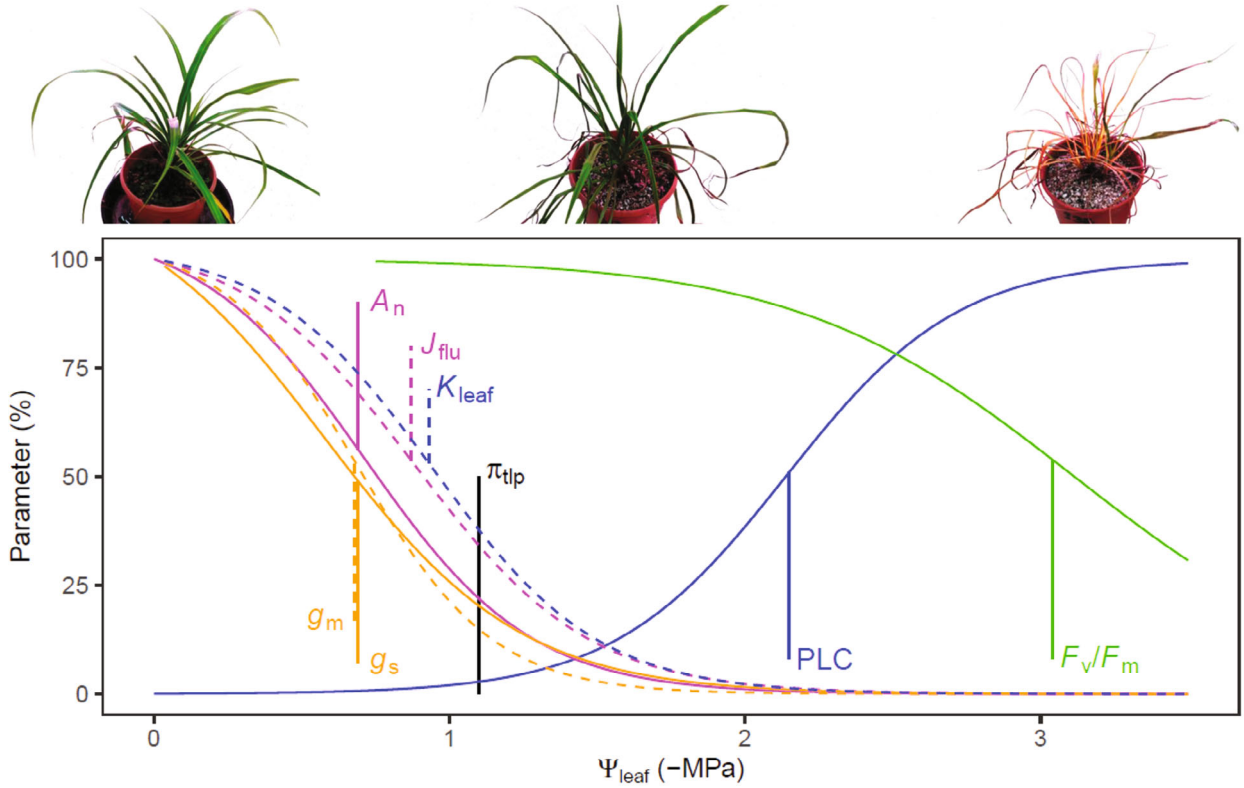

FIGURE 5 Sequence of events during leaf dehydration. Photosynthesis and hydraulic parameters are expressed as relative change in each parameter along with decreasing leaf water potential (Ψ_{leaf}). The included parameters are net CO_2 assimilation (A_n; solid red line), electron transport rate (J_{flu}; dashed red line), stomatal conductance (g_s; solid orange line), mesophyll conductance to CO_2 (g_m; dashed orange line), leaf hydraulic conductance measured in vivo with the evaporative flux method (K_{leaf}; dashed blue line), percentage loss of hydraulic conductivity calculated using theoretical hydraulic conductivity (k_h^{th}) from microCT images (PLC; solid blue line), and maximum yield of PSII (F_v/F_m; solid green line). The curves correspond to the sigmoidal fittings for each parameter shown in Figure 4. Vertical lines indicate the Ψ_{leaf} at which a given parameter declines by 50% (P_{50} corresponds to PLC at 50% decline). The black vertical line indicates the turgor loss point (π_{tlp}). The upper images show *B. purpurea* plants at different stages of water stress: well-watered conditions (left), turgor loss point and gas exchange cessation (middle), and desiccated state when chlorophyll is lost and RWC reaches ~10% (right).

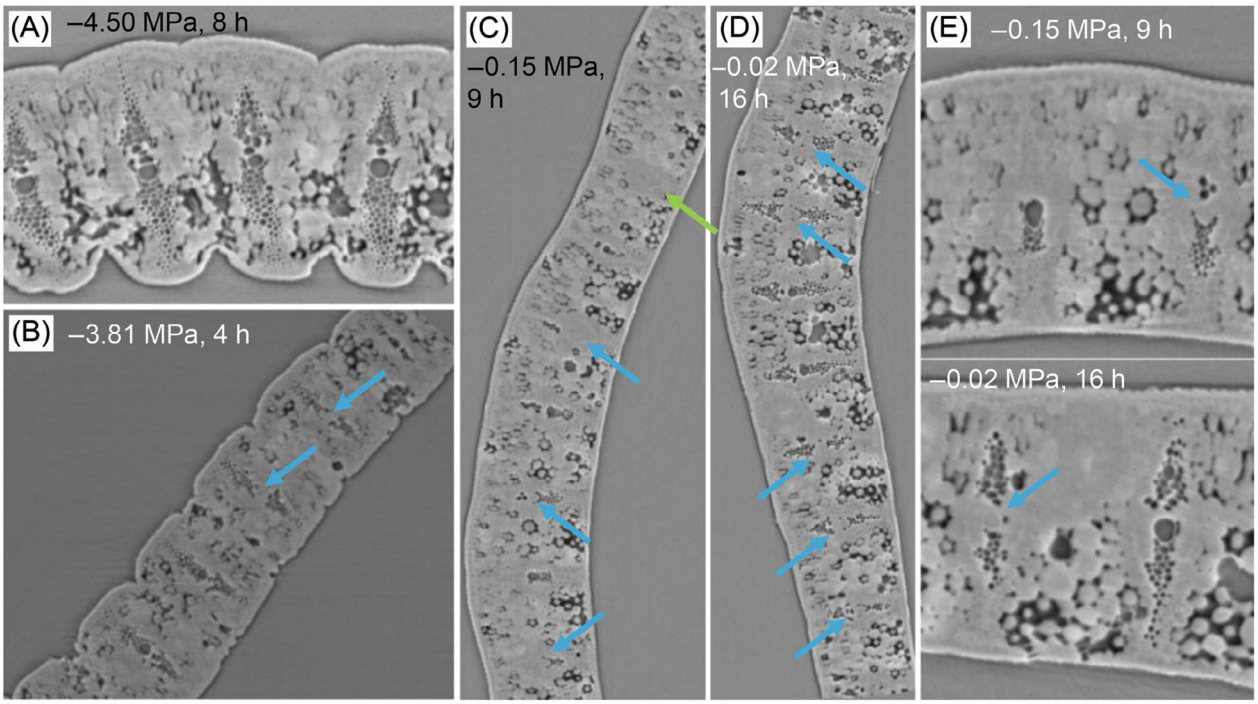

FIGURE 6 Leaf rehydration dynamics from x-ray microCT images. (A–D) Four representative leaves are shown at 4–16 h after rewatering. Each image includes the time since rewatering (hours) and the leaf water potential (Ψ_{leaf}). Refilled major vessels are indicated with blue arrows, and complete vascular bundle recovery (refilling of major and minor vessels) with a green arrow (only one bundle in C). (E) Detail of vascular bundles from leaves displayed in (C) and (D). Note the complete embolism and leaf shrinkage in (A) and the beginning of parenchyma rehydration and expansion in (B). (C) and (D) show how the parenchyma is fully hydrated, and mesophyll cells are completely expanded; however, vascular refilling is partial, as some of the xylem vessels are still embolised.

Embolism events evaluated from microCT images were detected from the onset of cavitation events to the full embolization of the xylem (Figure 3). The first events of embolism (P_{12}) occurred at −1.61 MPa and P_{50} and P_{88} were reached at −2.15 and −2.60 MPa, respectively (Table S1).

The response of photosynthetic parameters and K_{leaf} against Ψ_{leaf} and RWC (Figure 4) drives the sequence of events leading to photosynthesis and transpiration decline upon water stress (Figure 5; Table S1). The 50% decline of A_n, g_{sc}, g_m, J_{flu}, and K_{leaf} occurred at considerably high values of Ψ_{leaf} (−0.68 to −0.93 MPa). For K_{leaf}, both attached and excised leaves showed a similar Ψ_{leaf} at 50% decrease (−0.93 and − 0.81 MPa, respectively; Figures 4I and S1). A_n, g_s and g_m reached 88% decline at slightly higher Ψ_{leaf} (−1.16 to −1.28 MPa) than J_{flu} and K_{leaf} (−1.54 MPa for both), coinciding with π_{tlp} (−1.10 ± 0.03 MPa). On the other hand, PLC increased only after almost complete cessation of A_n, g_{sc}, g_m, J_{flu}, and K_{leaf} (Figure 5). The difference between the water potential at 88% g_s decline (a proxy to stomatal closure) and P_{12} (the xylem pressure at the onset of embolism) yielded a positive stomatal safety margin of 0.43 MPa. F_v/F_m decrease is the last event of the sequence, where F_v/F_m <0.50 occurred after full embolism at approximately −3 MPa. When considering the sequence in terms of RWC, the 88% decline in all photosynthesis parameters, K_{leaf}, and the onset of embolism (P_{12}) occurred in the 85%–90% RWC range (Table S1), after the RWC_{tlp} (92%), whereas F_v/F_m remained high (F_v/F_m > 0.5) until reaching 70% RWC (Figure 4L).

3.2 | Plant rehydration dynamics

The rehydration of the plants after 21 days of water deprivation led to a rapid recovery from the desiccated state to control water status values, and even higher in the case of Ψ_{leaf} (−0.14 ± 0.01 MPa), within the first day of recovery (i.e., the first 24 h after rewatering; Figure 1B). Gas exchange parameters also recovered within the first few days after rewatering (Figure 2A–D). Thus, A_n, g_{sc}, and J_{flu} reached control values on the 3rd day while g_m recovered to initial values by the 2nd day after rehydration, although it did not achieve its maximum until the 7th day (Figure 2D). K_{leaf} reached the highest values on the first day of recovery, 20.9 ± 4.1 mmol H_2O m^{-2} s^{-1} MPa^{-1}, 2-fold higher than initial well-watered plants, and strongly decreased on the second day (Figure 2F). In the following days (3rd–7th), K_{leaf} experienced a gradual increase. Overall, all parameters reached similar values to those prior to water stress 1 week after rewatering.

The dynamics of the partial recovery of the hydraulic functioning can be observed in Figure 6. Leaf mesophyll fully rehydrated and expanded (reaching Ψ_{leaf} close to 0 MPa) within 9–16 h in some cases (Figure 6C,D). However, at that stage, some of the vessels were still

air-filled and approximately half of the observed vascular bundles showed recovery in the central vessel (Figure 6C,D).

4 | DISCUSSION

B. purpurea showed a coordinated decline in photosynthesis functioning, stomatal conductance, and K_{leaf}, which preceded leaf xylem embolism. Notably, these events occurred prior to the dehydration levels that trigger extensive desiccation-tolerant mechanisms reported for this species (RWC of 50%–70%), such as starch mobilization and chlorophyll degradation (Suguiyama et al., 2014, 2016). From the microCT images during the first hours of recovery, we observed a relatively rapid (9–16 h) rehydration of the leaf mesophyll but an incomplete refilling of the vascular bundles which, together with photosystem reassembling, possibly limits the recovery of photosynthesis in the first 1–2 days after rewatering.

4.1 | Photosynthesis dynamics under dehydration

Photosynthesis decline in *B. purpurea* during dehydration resulted from a concomitant reduction in CO_2 availability driven by decreasing g_s and g_m, and photochemical limitations in the form of reduced J_{flu}. These three factors declined simultaneously when leaves reached −1 MPa, approximately (Figures 4 and 5). This combined decline in CO_2 diffusion and photochemical quenching at relatively high water content is a common response among desiccation-sensitive species (Nadal & Flexas, 2019; Trueba et al., 2019). In other resurrection species, including the homoiochlorophyllous angiosperms *Ramonda myconi*, *Craterostigma plantagineum*, and *Haberlea rhodopensis* (Peeva & Cornic, 2009; Schwab et al., 1989), photosynthesis decreases due to diffusion limitations instead of the shutdown of the photosynthetic apparatus, although photoinhibition has been observed in some cases (Rapparini et al., 2015). Chlorophyll degradation in poikilochlorophyllous plants occurs at the last stages of dehydration, under severe stress (Fernández-Marín et al., 2016). This is also true for *B. purpurea*, where chlorophyll *a* and *b* degradation has been reported long after photosynthesis cessation and RWC below 40% (Aidar et al., 2010; Suguiyama et al., 2014). Here, strong photosynthesis decrease (P_{88}) occurred at −1.28 MPa (90% RWC), well before chlorophyll degradation, which can be inferred from F_v/F_m decrease, which declined by 12% at −2.32 MPa and 91% RWC (Table S1). Hence, the causes of photosynthesis shutdown in *B. purpurea* are not driven by the desiccation tolerance mechanisms. Overall, it appears that photosynthesis response to drought in *B. purpurea* is similar to that of non-resurrection species.

The coupling of photosynthesis with the leaf hydraulic functioning has been scarcely reported for resurrection species, with only some recent studies in resurrection ferns (Nadal et al., 2021b; Prats & Brodersen, 2021) and a woody angiosperm (Fu et al., 2022). For *B. purpurea*, concomitant to g_s and g_m decrease, K_{leaf} experienced a similar reduction at the first stages of dehydration. A reduction in K_{leaf} leads to stomatal closure through reduced guard cell turgor (Rodríguez-Domínguez et al., 2016) and is related to both g_s and g_m decline under water stress (Flexas et al., 2018; Wang et al., 2018). The water pathway inside leaves can be decomposed into two components, the xylem described by K_x, and the outside-xylem (K_{ox}) pathways, which together define K_{leaf} (see Xiong & Nadal, 2020 and references therein). In *B. purpurea*, as K_{leaf} decline occurred prior to the onset of leaf xylem embolism (Figure 5), most of the hydraulic reduction could be attributed to the outside-xylem pathway conductance (K_{ox}), which is more sensitive to dehydration (Trueba et al., 2019), rather than xylem pathway conductance loss (K_x). The reduction in K_{ox} has been attributed to leaf shrinkage and decreased membrane conductivity (Scoffoni et al., 2014; Scoffoni et al., 2017). As lipid composition of membranes changes in the desiccated state and leaf shrinkage is a key feature among resurrection plants (Fernández-Marín et al., 2016), these species may constitute good candidates to test the causes of K_{ox} decrease under dehydration.

4.2 | Embolism formation and coordination with stomata

The observed dynamics in g_s and embolism formation during plant dehydration demonstrate the occurrence of embolism only after stomatal closure in *B. purpurea*. This coincides with previous findings from Aidar et al. (2010) reporting early stomatal closure in *B. purpurea* before reaching the desiccated state, and the response of most desiccation-sensitive species (Brodribb & McAdam, 2017; Creek et al., 2020). In this study, g_s decline by 88% occurred at slightly higher Ψ_{leaf} (−1.18 MPa) than the onset of embolism (P_{12} of −1.61 MPa; Table S1). However, these results contrast with what may a priori be expected from resurrection plants. For instance, Sherwin et al. (1998) suggested that stomatal closure occurred during the bulk of embolism events in the stem in *Myrothamnus flabellifolius*, allowing this species to "maximize carbon gain" during dehydration. Nonetheless, the response of stomata—and hence photosynthesis—appears to be far from homogeneous among resurrection plants (Fernández-Marín et al., 2016). For instance, *Eragrostis nindensis*, *Craterostigma wilmsii*, *M. flabellifolius*, and *Haberlea rhodopensis* are able to keep stomata open and positive A_n as far as to RWC < 50% (Farrant, 2000; Willigen et al., 2001), whereas in *Xerophyta humilis* photosynthesis ceased at RWC ~80% (Beckett et al., 2012). The differential response may be related to the adoption of poikilochlorophylly (Fernández-Marín et al., 2016). In this sense, stomatal closure could reduce the dehydration rate and allow for additional time to complete the needed protection mechanisms (Aidar et al., 2010). In our study, stomatal closure occurred by the 11th day after water deprivation (Figure 2B) but RWC did not decrease below 70% until the 18th day (Figure 1B). Full xylem embolism occurred within the timelapse comprised between stomatal closure and RWC steep decrease (Figures 1 and 2), simultaneous to gradual loss of F_v/F_m (Figure 5). According to Trueba et al. (2019), even slight losses in F_v/F_m (decline by 10%) in desiccation-sensitive species indicate that leaves are not able to recover after

dehydration. This pattern, where leaf embolism leads to dehydration, indicated by leaf shrinkage and/or F_v/F_m decline of the surrounding mesophyll tissue (Brodribb et al., 2021; Johnson et al., 2022), also occurs in *B. purpurea* (Figure 5). However, in this case, the immediate decrease in water content does not lead to cell death but possibly triggers the cascade of protective mechanisms at the cell level, including starch mobilization, chlorophyll degradation, and sucrose and raffinose accumulation (Suguiyama et al., 2014).

Given the coordination of stomatal closure and leaf embolism found in *B. purpurea* and reported in other species (Cardoso et al., 2018; Creek et al., 2020; Hochberg et al., 2017), a relatively high embolism resistance in resurrection plants would allow to sustain carbon gain under progressive water stress. However, when comparing the P_{50} of *B. purpurea* (−2.15 MPa) to the reported values for leaves in other species, this species does not present higher resistance than, for example, oaks (mean leaf P_{50} of −3.8 MPa across 8 Mediterranean species; Skelton et al. (2018)) nor other woody angiosperms (mean P_{50} of −5.2 in three species; Creek et al. (2020)). For instance, the P_{50} of *B. purpurea* was similar to that reported in wheat leaves of −2.21 MPa (Corso et al. (2020) and the relatively drought-sensitive *Populus tremula x alba* of −1.96 MPa (Mantova et al. (2023). On the other hand, *B. purpurea* shows a small leaf safety margin (0.4 MPa) compared to >2 MPa in some woody evergreens (Creek et al., 2020). This may reflect the decreased need to prevent leaf damage due to dehydration in a resurrection plant since larger safety margins are related to reduced leaf and plant mortality rates under drought conditions (Chen et al., 2019; Creek et al., 2020).

4.3 | Hydraulic and photosynthesis recovery during rewatering

B. purpurea leaves were able to recover from drought and reach similar water status as control plants (i.e., $\Psi_{leaf} \approx 0$ MPa and RWC ≈ 100%) within less than 24 h after being rewatered from the roots only (Figure 1B). Mesophyll tissue appeared to be fully rehydrated in some leaves even within the 9–16 h range (Figure 6). However, for the same leaves, the majority of vessels remained embolized, with a high degree of variability regarding the refilling of major and minor vessels (Figure 6E). Among the images obtained from microCT for rehydrated leaves, only one vascular bundle appeared fully recovered, with complete refilling in all major and minor vessels (Figure 6C), which is nonetheless still remarkable after complete embolism in the desiccated state (Figures 3C and 6A). A similar degree of embolism in all vessels has been shown in the petioles and stipes of resurrection ferns in the desiccated state (Holmlund et al., 2019; Prats & Brodersen, 2021). In fern petioles, xylem refilling occurs after rehydration of the surrounding living chlorenchyma and phloem (Holmlund et al., 2019, 2020). Similarly, for the leaves in *B. purpurea*, we observe rehydration of the surrounding tissues like bundle sheath and mesophyll cells in the first stage of rewatering. The role that these tissues may exert in aiding the refilling of the vessels is unclear, although it has been suggested that they may provide an increased osmotic gradient that contributes to water distribution in the xylem (Holmlund et al., 2019). Both positive root pressure and water ascension by capillarity have been suggested as two possible mechanisms for rehydration in desiccation-sensitive (e.g., Charrier et al., 2016) and resurrection plants (Holmlund et al., 2020; Schneider et al., 2000; Sherwin et al., 1998), although in the latter these mechanisms have been only explored in the stems of *M. flabellifolius* and the rachis of resurrection ferns.

Regarding photosynthesis recovery, A_n requires 3–4 days to reach pre-stressed values (Figure 2A), similar to what Fu et al. (2022) reported in the woody angiosperm *Paraboea rufescens*. The resynthesis of chlorophyll and photosystems assembly occurs in 24–48 h in *B. purpurea*, as reflected by the increase in F_v/F_m (Figure 2E), a similar timeframe (12–36 h) to that reported by Suguiyama et al. (2014). The biochemical limitations imposed by the reassembling of the photosynthetic pigments, together with xylem refilling, explain the lower photosynthesis in *B. purpurea* during the second to third day after rewatering (Figure 2A). Similar to the dehydration phase, the recovery of g_s, g_m, and J_{flu} was coordinated with A_n after rewatering (Figure 2). The slight delay of photosynthesis recovery compared to the full hydration within the first 24 h (Figure 1B) corresponds to the first stages of chlorophyll resynthesis (Suguiyama et al., 2014), as reflected by the extremely low F_v/F_m during the first day of recovery (Figure 2E) despite the high leaf hydrated status (Figure 4K,L). Additionally, photosynthesis recovery could also be hindered by stomatal shutdown due to residual effects of ABA accumulation during desiccation (McAdam & Brodribb, 2012), since ABA is a key regulator of desiccation tolerance (Oliver et al., 2020). In contrast to *B. purpurea*, Prats and Brodersen (2021) reported relatively rapid photosynthesis recovery in *P. polypodioides* within 12 h. In this fern, photosynthesis recovered despite uncomplete xylem refilling due to the decoupling between leaf and rhizome, which the authors attributed to the relevance of foliar water uptake for rapid recovery, probably linked to its epiphytic environment (Prats & Brodersen, 2021). Similarly, the desiccation-tolerant fronds of *Anemia caffrorum* require high relative humidity in the atmosphere to recover from the desiccated state and are able to resume photosynthesis within the first 24 h after rewatering (Nadal et al., 2021b). However, resurrection ferns may not provide a comparable system for *B. purpurea*, since the latter must reassemble its photosynthetic apparatus during recovery.

Notably, K_{leaf} shows an extreme value in the first day of recovery (Figure 2F), and then decreases to approximately pre-stressed values in the following days. Since most vessels are still embolized during the first 24 h after rewatering (Figure 6), and K_{leaf} is thought to reflect both xylem and outside-xylem water pathways, it seems that this high value may constitute an artifact product of the measurement technique. The evaporative flux method requires measurements of transpiration and water potential differences. However, at such low E (0.52 mmol m^{-2} s^{-1} on day R1) and Ψ_{leaf} and Ψ_{stem} (−0.14 and − 0.11 MPa, respectively), the measurement noise might outweigh the signal. Nonetheless, the response of K_{leaf} to Ψ_{leaf} is very similar for both dehydrating and rehydrating leaves, with K_{leaf} presenting maximum values at the lowest Ψ_{leaf} in both stages (Figure 4L). The decoupling of K_{leaf} and embolism dynamics in *B. purpurea* may indicate

that K_{leaf} is more related to K_{ox} than to K_x. Further exploration of hydraulic conductance in resurrection, preferably with comparison to other methods for measuring K_{leaf} (Flexas et al., 2013), may help in disentangling the role of the two pathways during leaf rehydration.

5 | CONCLUSIONS

This study shows for the first time the detailed interplay between photosynthesis, hydraulic conductance, and xylem embolism during dehydration and rehydration in a resurrection plant. As expected, photosynthesis decreased due to a combination of stomatal closure and declines in mesophyll conductance and electron transport. This occurred at a relatively low level of water stress compared to the degree of dehydration experienced by *B. purpurea* and other resurrection plants (Oliver et al., 2020). This response constitutes a common pattern across vascular plants for photosynthesis decline under drought conditions (Flexas et al., 2018; Nadal & Flexas, 2019). *B. purpurea* did not show remarkably low leaf P_{50} values (−2.15 MPa), showing lower resistance to embolism than woody angiosperm species (e.g., Creek et al., 2020; Skelton et al., 2018). Also, photosynthesis in *B. purpurea* recovered within a few days after rewatering, after chlorophyll resynthesis, indicated by the recovery of F_v/F_m, and simultaneous to the resuming of hydraulic function. Notably, stomatal closure and photosynthesis cessation occurred prior to xylem embolism as in most desiccation-sensitive species, adding evidence to the view that stomata act as "safety valves" to protect the vascular system from embolism formation. The fact that a resurrection plant, with no a priori need for embolism protection, still displays such behavior points toward a conserved response of stomata during drought across vascular plants. Nonetheless, as *B. purpurea* presents the most derived strategy among resurrection plants (poikilochlorophylly), the study of other resurrection plants with the homoiochlorophyllous strategy may help us to further disentangle the dynamics of carbon gain and hydraulics in this remarkable group of plants.

AUTHOR CONTRIBUTIONS

Miquel Nadal, Marc Carriquí, Jaume Flexas, and José M. Torres-Ruiz designed the research. Miquel Nadal, Marc Carriquí, Eric Badel, Hervé Cochard, Sylvain Delzon, Andrew King, Laurent J. Lamarque, and José M. Torres-Ruiz performed the research. Miquel Nadal, Marc Carriquí, and José M. Torres-Ruiz discussed and interpreted the data. Miquel Nadal drafted the first version and all authors contributed to the final writing, review, and editing of the manuscript.

ACKNOWLEDGMENTS

This work was supported by the project PGC2018-093824-B-C41 from the Ministerio de Ciencia, Innovación y Universidades (Spain), the European Regional Development Fund (ERDF), and La Région Auvergne-Rhône-Alpes "Pack Ambition International 2020" through the project "*ThirsTree*" 20-006175-01, 20-006175-02. MN was supported by the predoctoral fellowship BES-2015-072578, financed by the Ministerio de Economía y Competitividad (MINECO) and the European Social Fund; and the postdoctoral fellowships Juan de la Cierva-Formación (FJC2020-043902-I and FJC2020-042856-I), financed by MCIN/AEI/10.13039/501100011033 (Spain) and the European Union ("NextGenerationEU/PRTR"). We thank Dra. Alicia V. Perera Castro for her help in figure preparation.

DATA AVAILABILITY STATEMENT

Data sharing is not applicable to this article as all newly created data are already contained within this article.

ORCID

Miquel Nadal https://orcid.org/0000-0003-1472-1792
Marc Carriquí https://orcid.org/0000-0002-0153-2602
Eric Badel https://orcid.org/0000-0003-2282-7554
Hervé Cochard https://orcid.org/0000-0002-2727-7072
Sylvain Delzon https://orcid.org/0000-0003-3442-1711
Laurent J. Lamarque https://orcid.org/0000-0002-1430-5193
Jaume Flexas https://orcid.org/0000-0002-3069-175X
José M. Torres-Ruiz https://orcid.org/0000-0003-1367-7056

REFERENCES

Aidar, S.T., Meirelles, S.T., Oliveira, R.F., Chaves, A.R.M. & Fernandes-Júnior, P.I. (2014) Photosynthetic response of poikilochlorophyllous desiccation-tolerant *Pleurostima purpurea* (Velloziaceae) to dehydration and rehydration. *Photosynthetica*, 52(1), 124–133.

Aidar, S.T., Meirelles, S.T., Pocius, O., Delitti, W.B.C., Souza, G.M. & Gonçalves, A.N. (2010) Desiccation tolerance in *Pleurostima purpurea* (Velloziaceae). *Plant Growth Regulation*, 62(3), 193–202.

Alpert, P. (2005) The limits and frontiers of desiccation-tolerant life. *Integrative and Comparative Biology*, 45(5), 685–695.

Bartlett, M.K., Klein, T., Jansen, S., Choat, B. & Sack, L. (2016) The correlations and sequence of plant stomatal, hydraulic, and wilting responses to drought. *Proceedings of the National Academy of Sciences of the United States of America*, 113(46), 13098–13103.

Beckett, M., Loreto, F., Velikova, V., Brunetti, C., Di Ferdinando, M., Tattini, M. et al. (2012) Photosynthetic limitations and volatile and non-volatile isoprenoids in the poikilochlorophyllous resurrection plant *Xerophyta humilis* during dehydration and rehydration. *Plant, Cell & Environment*, 35(12), 2061–2074.

Bellasio, C., Beerling, D.J. & Griffiths, H. (2016) An Excel tool for deriving key photosynthetic parameters from combined gas exchange and chlorophyll fluorescence: theory and practice. *Plant, Cell & Environment*, 39(6), 1180–1197.

Brodribb, T., Brodersen, C.R., Carriquí, M., Tonet, V., Rodríguez-Domínguez, C. & McAdam, S. (2021) Linking xylem network failure with leaf tissue death. *New Phytologist*, 232(1), 68–79.

Brodribb, T.J. & McAdam, S.A.M. (2017) Evolution of the stomatal regulation of plant water content. *Plant Physiology*, 174(2), 639–649.

Cardoso, A.A., Brodribb, T.J., Lucani, C.J., DaMatta, F.M. & McAdam, S. A.M. (2018) Coordinated plasticity maintains hydraulic safety in sunflower leaves. *Plant, Cell & Environment*, 41(11), 2567–2576.

Charrier, G., Torres-Ruiz, J.M., Badel, E., Burlett, R., Choat, B., Cochard, H., et al. (2016) Evidence for hydraulic vulnerability segmentation and lack of xylem refilling under tension. *Plant Physiology*, 172, 1657–1668.

Chaves, M.M., Flexas, J. & Pinheiro, C. (2009) Photosynthesis under drought and salt stress: regulation mechanisms from whole plant to cell. *Annals of Botany-London*, 103(4), 551–560.

Chen, Z., Li, S., Luan, J., Zhang, Y., Zhu, S., Wan, X. et al. (2019) Prediction of temperate broadleaf tree species mortality in arid limestone habitats with stomatal safety margins. *Tree Physiology*, 39(8), 1428–1437.

Choat, B., Badel, E., Burlett, R., Delzon, S., Cochard, H. & Jansen, S. (2016) Noninvasive measurement of vulnerability to drought-induced embolism by x-ray microtomography. *Plant Physiology*, 170(1), 273–282.

Corso, D., Delzon, S., Lamarque, L.J., Cochard, H., Torres-Ruiz, J.M., King, A. et al. (2020) Neither xylem collapse, cavitation, or changing leaf conductance drive stomatal closure in wheat. *Plant, Cell & Environment*, 43(4), 854–865.

Creek, D., Lamarque, L.J., Torres-Ruiz, J.M., Parise, C., Burlett, R., Tissue, D.T. et al. (2020) Xylem embolism in leaves does not occur with open stomata: evidence from direct observations using the optical visualization technique. *Journal of Experimental Botany*, 71(3), 1151–1159.

Duursma, R.A. & Choat, B. (2017) Fitplc—an R package to fit hydraulic vulnerability curves. *Journal of Plant Hydraulics*, 4, e-002.

Evans, J.R., Kaldenhoff, R., Genty, B. & Terashima, I. (2009) Resistances along the CO_2 diffusion pathway inside leaves. *Journal of Experimental Botany*, 60(8), 2235–2248.

Farrant, J.M. (2000) A comparison of mechanisms of desiccation tolerance among three angiosperm resurrection plant species. *Plant Ecology*, 151, 29–39.

Farrant, J.M. & Moore, J.P. (2011) Programming desiccation-tolerance: from plants to seeds to resurrection plants. *Current Opinion in Plant Biology*, 14(3), 340–345.

Fernández-Marín, B., Holzinger, A. & García-Plazaola, J.I. (2016) Photosynthesis strategies of desiccation-tolerant organisms. In: Pessarakli, M. (Ed.) *Handbook of photosynthesis*. Boca Raton, FL: CRC Press, pp. 663–681.

Flexas, J., Bota, J., Loreto, F., Cornic, G. & Sharkey, T.D. (2004) Diffusive and metabolic limitations to photosynthesis under drought and salinity in C(3) plants. *Plant Biology*, 6(3), 269–279.

Flexas, J., Carriquí, M. & Nadal, M. (2018) Gas exchange and hydraulics during drought in crops: who drives whom? *Journal of Experimental Botany*, 69(16), 3791–3795.

Flexas, J., Díaz-Espejo, A., Berry, J.A., Cifre, J., Galmés, J., Kaldenhoff, R. et al. (2007) Analysis of leakage in IRGA's leaf chambers of open gas exchange systems: quantification and its effects in photosynthesis parameterization. *Journal of Experimental Botany*, 58(6), 1533–1543.

Flexas, J., Ribas-Carbo, M., Diaz-Espejo, A., Galmes, J. & Medrano, H. (2008) Mesophyll conductance to CO_2: current knowledge and future prospects. *Plant, Cell & Environment*, 31(5), 602–621.

Flexas, J., Scoffoni, C., Gago, J. & Sack, L. (2013) Leaf mesophyll conductance and leaf hydraulic conductance: an introduction to their measurement and coordination. *Journal of Experimental Botany*, 64(13), 3965–3981.

Fu, P.L., Zhang, Y., Zhang, Y.J., Finnegan, P.M., Yang, S.J. & Fan, Z.X. (2022) Leaf gas exchange and water relations of the woody desiccation-tolerant *Paraboea rufescens* during dehydration and rehydration. *AoB Plants*, 14(4), plac033.

Gaff, D.F. & Oliver, M. (2013) The evolution of desiccation tolerance in angiosperm plants: a rare yet common phenomenon. *Functional Plant Biology*, 40(4), 315–328.

Gago, J., Carriquí, M., Nadal, M., Clemente-Moreno, M.J., Coopman, R.E., Fernie, A.R. et al. (2019) Photosynthesis optimized across land plant phylogeny. *Trends in Plant Science*, 24(10), 947–958.

Galmés, J., Conesa, M.À., Ochogavia, J.M., Perdomo, J.A., Francis, D.M., Ribas-Carbó, M. et al. (2011) Physiological and morphological adaptations in relation to water use efficiency in Mediterranean accessions of *Solanum lycopersicum*. *Plant, Cell & Environment*, 34(2), 245–260.

Galmés, J., Medrano, H. & Flexas, J. (2006) Acclimation of Rubisco specificity factor to drought in tobacco: discrepancies between in vitro and in vivo estimations. *Journal of Experimental Botany*, 57(14), 3659–3667.

Galmés, J., Medrano, H. & Flexas, J. (2007) Photosynthetic limitations in response to water stress and recovery in Mediterranean plants with different growth forms. *New Phytologist*, 175(1), 81–93.

Harley, P.C., Loreto, F., Di Marco, G. & Sharkey, T.D. (1992) Theoretical considerations when estimating the mesophyll conductance to CO_2 flux by analysis of the response of photosynthesis to CO_2. *Plant Physiology*, 98(4), 1429–1436.

Hoagland, D.R. & Arnon, D.I. (1950) The water-culture method for growing plants without soil. Circular California agricultural experiment station, 3^{47} (2nd edit).

Hochberg, U., Windt, C.W., Ponomarenko, A., Zhang, Y.J., Gersony, J., Rockwell, F.E. et al. (2017) Stomatal closure, basal leaf embolism, and shedding protect the hydraulic integrity of grape stems. *Plant Physiology*, 174(2), 764–775.

Holmlund, H.I., Davis, S.D., Ewers, F.W., Aguirre, N.M., Sapes, G., Sala, A. et al. (2020) Positive root pressure is critical for whole-plant desiccation recovery in two species of terrestrial resurrection ferns. *Journal of Experimental Botany*, 71(3), 1139–1150.

Holmlund, H.I., Pratt, R.B., Jacobsen, A.L., Davis, S.D. & Pittermann, J. (2019) High-resolution computed tomography reveals dynamics of desiccation and rehydration in fern petioles of a desiccation-tolerant fern. *New Phytologist*, 224(1), 97–105.

Hsiao, T.C., Acevedo, E., Ferreres, E. & Henderson, D.W. (1976) Water stress, growth and osmotic adjustment. *Philosophical Transactions of the Royal Society of London B, Biological Sciences*, 273(927), 479–500.

Johnson, K.M., Lucani, C. & Brodribb, T.J. (2022) In vivo monitoring of drought-induced embolism in *Callitris rhomboidea* trees reveals wide variation in branchlet vulnerability and high resistance to tissue death. *New Phytologist*, 233(1), 207–218.

King, A., Guignot, N., Zerbino, P., Boulard, E., Desjardins, K., Bordessoule, M. et al. (2016) Tomography and imaging at the PSICHE beam line of the SOLEIL synchrotron. *Review of Scientific Instruments*, 87(9), 093704.

Lens, F., Gleason, S.M., Bortolami, G., Brodersen, C., Delzon, S. & Jansen, S. (2022) Functional xylem characteristics associated with drought-induced embolism in angiosperms. *New Phytologist*, 236(6), 2019–2036.

Mantova, M., Cochard, H., Burlett, R., Delzon, S., King, A., Rodriguez-Dominguez, C.M. et al. (2023) On the path from xylem hydraulic failure to downstream cell death. *New Phytologist*, 237(3), 793–806.

Mantova, M., Herbette, S., Cochard, H. & Torres-Ruiz, J.M. (2022) Hydraulic failure and tree mortality: from correlation to causation. *Trends in Plant Science*, 27(4), 335–345.

Martin-StPaul, N., Delzon, S. & Cochard, H. (2017) Plant resistance to drought depends on timely stomatal closure. *Ecology Letters*, 20(11), 1437–1447.

McAdam, S.A. & Brodribb, T.J. (2012) Fern and lycophyte guard cells do not respond to endogenous abscisic acid. *Plant Cell*, 24(4), 1510–1521.

Meireles, S.T., de Mattos, E.A. & da Silva, A.C. (1997) Potential desiccation tolerant vascular plants from southeastern Brazil. *Polish Journal of Environmental Studies*, 6(4), 17–21.

Mirone, A., Brun, E., Gouillart, E., Tafforeau, P. & Kieffer, J. (2014) The PyHST2 hybrid distributed code for high speed tomographic reconstruction with iterative reconstruction and a priori knowledge capabilities. *Nuclear Instruments and Methods in Physics Research Section B: Beam Interactions with Materials and Atoms*, 324, 41–48.

Nadal, M., Brodribb, T.J., Fernandez-Marin, B., Garcia-Plazaola, J.I., Arzac, M.I., Lopez-Pozo, M. et al. (2021b) Differences in biochemical, gas exchange and hydraulic response to water stress in desiccation tolerant and sensitive fronds of the fern *Anemia caffrorum*. *New Phytologist*, 231(4), 1415–1430.

Nadal, M. & Flexas, J. (2018) Mesophyll conductance to CO_2 diffusion: effects of drought and opportunities for improvement. In: *Water scarcity and sustainable agriculture in semiarid environment*. Cambridge, MA: Academic Press, pp. 403–438.

Nadal, M. & Flexas, J. (2019) Variation in photosynthetic characteristics with growth form in a water-limited scenario: implications for assimilation rates and water use efficiency in crops. *Agricultural Water Management*, 216, 457–472.

Nadal, M., Perera-Castro, A.V., Gulías, J., Farrant, J.M. & Flexas, J. (2021a) Resurrection plants optimize photosynthesis despite very thick cell walls by means of chloroplast distribution. *Journal of Experimental Botany*, 72(7), 2600–2610.

Oliver, M.J., Farrant, J.M., Hilhorst, H.W.M., Mundree, S., Williams, B. & Bewley, J.D. (2020) Desiccation tolerance: avoiding cellular damage during drying and rehydration. *Annual Review of Plant Biology*, 71, 435–460.

Oliver, M.J., Tuba, Z. & Mishler, B.D. (2000) The evolution of vegetative desiccation tolerance in land plants. *Plant Ecology*, 151(1), 85–100.

Oliver, M.J., Velten, J. & Mishler, B.D. (2005) Desiccation tolerance in bryophytes: a reflection of the primitive strategy for plant survival in dehydrating habitats? *Integrative and Comparative Biology*, 45(5), 788–799.

Paganin, D., Mayo, S.C., Gureyev, T.E., Miller, P.R. & Wilkins, S.W. (2002) Simultaneous phase and amplitude extraction from a single defocused image of a homogeneous object. *Journal of Microscopy*, 206(Pt 1), 33–40.

Peeva, V. & Cornic, G. (2009) Leaf photosynthesis of *Haberlea rhodopensis* before and during drought. *Environmental and Experimental Botany*, 65(2–3), 310–318.

Perera-Castro, A.V., Nadal, M. & Flexas, J. (2020) What drives photosynthesis during desiccation? Mosses and other outliers from the photosynthesis-elasticity trade-off. *Journal of Experimental Botany*, 71(20), 6460–6470.

Porembski, S. (2011) Evolution, diversity, and habitats of poikilohydrous vascular plants. In: Lüttge, U., Beck, E. & Bartels, D. (Eds.) *Plant desiccation tolerance. Ecological studies*. Berlin, Heidelberg: Springer, pp. 139–156.

Prats, K.A. & Brodersen, C.R. (2021) Desiccation and rehydration dynamics in the epiphytic resurrection fern *Pleopeltis polypodioides*. *Plant Physiology*, 187(3), 1501–1518.

R Core Team. (2022) *R: a language and environment for statistical computing*. Vienna, Austria: R Foundation for Statistical Computing. Available at: https://www.R-project.org/

Rapparini, F., Neri, L., Mihailova, G., Petkova, S. & Georgieva, K. (2015) Growth irradiance affects the photoprotective mechanisms of the resurrection angiosperm *Haberlea rhodopensis* Friv. in response to desiccation and rehydration at morphological, physiological and biochemical levels. *Environmental and Experimental Botany*, 113, 67–79.

Rodríguez-Domínguez, C.M., Buckley, T.N., Egea, G., de Cires, A., Hernández-Santana, V., Martorell, S. et al. (2016) Most stomatal closure in woody species under moderate drought can be explained by stomatal responses to leaf turgor. *Plant, Cell & Environment*, 39(9), 2014–2026.

Sack, L. & Pasquet-Kok, J. (2011) Leaf pressure-volume curve parameters. PrometheusWiki. Available at: http://prometheuswiki.org/tiki-pagehistory.php?page=Leaf%20pressure-volume%20curve%20parameters&preview=16. Last accessed 12 October 2022

Sack, L. & Scoffoni, C. (2011) Minimum epidermal conductance (gmin, a.k.a. cuticular conductance). PrometheusWiki. Available at: http://prometheuswiki.org/tiki-pagehistory.php?page=Minimum%20epidermal%20conductance%20(gmin,%20a.k.a.%20cuticular%20conductance)&preview=7. Last accessed 12 October 2022

Sack, L. & Scoffoni, C. (2012) Measurement of leaf hydraulic conductance and stomatal conductance and their responses to irradiance and dehydration using the evaporative flux method (EFM). *Journal of Visualized Experiments*, 70, 4179.

Savi, T., Marin, M., Luglio, J., Petruzzellis, F., Mayr, S. & Nardini, A. (2016) Leaf hydraulic vulnerability protects stem functionality under drought stress in *Salvia officinalis*. *Functional Plant Biology*, 43(4), 370–379.

Schneider, H., Wistuba, N., Wagner, H.J., Thurmer, F. & Zimmermann, U. (2000) Water rise kinetics in refilling xylem after desiccation in a resurrection plant. *New Phytologist*, 148(2), 221–238.

Schneider, C.A., Rasband, W.S. & Eliceiri, K.W. (2012) NIH Image to ImageJ: 25 years of image analysis. *Nature Methods*, 9(7), 671–675.

Schwab, K.B., Schreiber, U. & Heber, U. (1989) Response of photosynthesis and respiration of resurrection plants to desiccation and rehydration. *Planta*, 177(2), 217–227.

Scoffoni, C., Albuquerque, C., Brodersen, C.R., Townes, S.V., John, G.P., Bartlett, M.K. et al. (2017) Outside-xylem vulnerability, not xylem embolism, controls leaf hydraulic decline during dehydration. *Plant Physiology*, 173(2), 1197–1210.

Scoffoni, C., Vuong, C., Diep, S., Cochard, H. & Sack, L. (2014) Leaf shrinkage with dehydration: coordination with hydraulic vulnerability and drought tolerance. *Plant Physiology*, 164(4), 1772–1788.

Sherwin, R.P., Pammenter, N.W., February, E., Willigen, C.V. & Farrant, J.M. (1998) Xylem hydraulic characteristics, water relations and wood anatomy of the resurrection plant *Myrothamnus flabellifolius* Welw. *Annals of Botany-London*, 81, 567–575.

Skelton, R.P., Brodribb, T.J., McAdam, S.A.M. & Mitchell, P.J. (2017) Gas exchange recovery following natural drought is rapid unless limited by loss of leaf hydraulic conductance: evidence from an evergreen woodland. *New Phytologist*, 215(4), 1399–1412.

Skelton, R.P., Dawson, T.E., Thompson, S.E., Shen, Y., Weitz, A.P. & Ackerly, D. (2018) Low vulnerability to xylem embolism in leaves and stems of North American oaks. *Plant Physiology*, 177(3), 1066–1077.

Spiess, A. (2018) propagate: Propagation of Uncertainty. R package version 1.0–6. Available at: https://CRAN.R-project.org/package=propagate

Suguiyama, V.F., Sanches, R.F.E., Meirelles, S.T., Centeno, D.C., da Silva, E.A. & Braga, M.R. (2016) Physiological responses to water deficit and changes in leaf cell wall composition as modulated by seasonality in the Brazilian resurrection plant *Barbacenia purpurea*. *South African Journal of Botany*, 105, 270–278.

Suguiyama, V.F., Silva, E.A., Meirelles, S.T., Centeno, D.C. & Braga, M.R. (2014) Leaf metabolite profile of the Brazilian resurrection plant *Barbacenia purpurea* Hook. (Velloziaceae) shows two time-dependent responses during desiccation and recovering. *Frontiers in Plant Science*, 5, 96.

Théroux Rancourt, G., Ethier, G. & Pepin, S. (2015) Greater efficiency of water use in poplar clones having a delayed response of mesophyll conductance to drought. *Tree Physiology*, 35(2), 172–184.

Torres-Ruiz, J.M., Díaz-Espejo, A., Pérez-Martín, A. & Hernández-Santana, V. (2015a) Role of hydraulic and chemical signals in leaves, stems and roots in the stomatal behaviour of olive trees under water stress and recovery conditions. *Tree Physiology*, 35(4), 415–424.

Torres-Ruiz, J.M., Jansen, S., Choat, B., McElrone, A.J., Cochard, H., Brodribb, T.J. et al. (2015b) Direct x-ray microtomography observation confirms the induction of embolism upon xylem cutting under tension. *Plant Physiology*, 167(1), 40–43.

Trifilò, P., Nardini, A., Lo Gullo, M.A., Barbera, P.M., Savi, T. & Raimondo, F. (2015) Diurnal changes in embolism rate in nine dry forest trees: relationships with species-specific xylem vulnerability, hydraulic strategy and wood traits. *Tree Physiology*, 35(7), 694–705.

Trueba, S., Pan, R., Scoffoni, C., John, G.P., Davis, S.D. & Sack, L. (2019) Thresholds for leaf damage due to dehydration: declines of hydraulic function, stomatal conductance and cellular integrity precede those for photochemistry. *New Phytologist*, 223(1), 134–149.

Tsuda, M. & Tyree, M.T. (2000) Plant hydraulic conductance measured by the high pressure flow meter in crop plants. *Journal of Experimental Botany*, 51(345), 823–828.

Tuba, Z. (2008) Notes on the poikilochlorophyllous desiccation-tolerant plants. *Acta Biologica Szegediensis*, 52(1), 111–113.

Wang, X., Du, T., Huang, J., Peng, S. & Xiong, D. (2018) Leaf hydraulic vulnerability triggers the decline in stomatal and mesophyll conductance during drought in rice. *Journal of Experimental Botany*, 69(16), 4033–4045.

Willigen, C.V., Pammenter, N.W., Mundree, S. & Farrant, J.M. (2001) Some physiological comparisons between the resurrection grass, *Eragrostis nindensis*, and the related desiccation-sensitive species, *E. curvula*. *Plant Growth Regulation*, 35, 121–129.

Wood, A.J. (2007) The nature and distribution of vegetative desiccation-tolerance in hornworts, liverworts and mosses. *The Bryologist*, 110(2), 163–177.

Xiong, D. & Nadal, M. (2020) Linking water relations and hydraulics with photosynthesis. *Plant Journal*, 101(4), 800–815.

Zufferey, V., Cochard, H., Ameglio, T., Spring, J.L. & Viret, O. (2011) Diurnal cycles of embolism formation and repair in petioles of grapevine (*Vitis vinifera* cv. Chasselas). *Journal of Experimental Botany*, 62(11), 3885–3894.

SUPPORTING INFORMATION

Additional supporting information can be found online in the Supporting Information section at the end of this article.

How to cite this article: Nadal, M., Carriquí, M., Badel, E., Cochard, H., Delzon, S., King, A. et al. (2023) Photosynthesis, leaf hydraulic conductance and embolism dynamics in the resurrection plant *Barbacenia purpurea*. *Physiologia Plantarum*, 175(5), e14035. Available from: https://doi.org/10.1111/ppl.14035